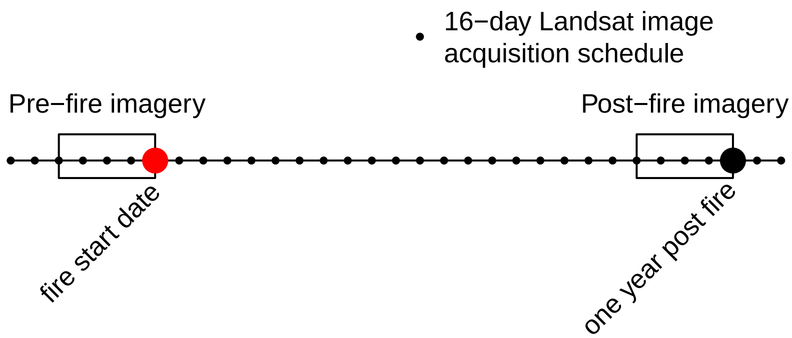

Figure 1: Schematic for how Landsat imagery was assembled in order to make comparisons between pre- and post-fire conditions. This schematic depicts a 64-day window of image collation prior to the fire which comprise the pre-fire image collection. A similar, 64-day window collection of imagery is assembled one year after the pre-fire image collection.

Supplemental methods

Normalized difference vegetation index (NDVI; Eq. 1) correlates with vegetation density, canopy cover, and leaf area index (1). Normalized difference moisture index (NDMI; Eq. 2) correlates with similar vegetation characteristics as NDVI, but doesn't saturate at high levels of foliar biomass (2). Normalized burn ratio (NBR; Eq. 3) and normalized burn ratio version 2 (NBR2; Eq. 4) respond strongly to fire effects on vegetation (4–8).

(1) $ndvi = (nir - red)/(nir + red)$

(2) $ndmi = (nir - swir1)/(nir + swir1)$

(3) $nbr = (nir - swir2)/(nir + swir2)$

(4) $nbr2 = (swir1 - swir2)/(swir1 + swir2)$

Where *nir* is the near infrared band (band 4 on Landsat 4, 5, and 7; band 5 on Landsat 8) and *red* is the red band (band 3 on Landsat 4, 5, and 7; band 4 on Landsat 8), $swir1$ is the first short wave infrared band (band 5 on Landsat 4, 5, and 7; band 4 on Landsat 8), $swir2$ is the second short wave infrared band (band 7 on Landsat 4, 5, 7, and 8)

We calculated the delta severity indices (dNBR, dNBR2, dNDVI) by subtracting the respective postfire indices from the prefire indices (NBR, NBR2, and NDVI) without multiplying by a rescaling constant (e.g., we did not multiply the result by 1000 as in (9); Eq. 5). Following (10), we chose not to correct the delta indices using a phenological offset value (typically calculated as the delta index in homogeneous forest patch outside of the fire perimeter), as our approach implicitly accounts for phenology by incorporating multiple cloud-free images across the same time window both before the fire and one year later.

(5) $dI = I_{\text{prefire}} - I_{\text{postfire}}$

We calculated the relative delta severity indices, RdNBR and RdNDVI, by scaling the respective delta indices (dNBR and dNDVI) from Eq. 6 by a square root transformation of the absolute value of the prefire index:

(6) $RdI = \frac{dI}{\sqrt{|I_{\text{prefire}}|}}$

We calculated the relative burn ratio (RBR) following (11) using Eq. 7:

(7) $RBR = \frac{dNBR}{NBR_{\text{prefire}}+1.001}$

We used the digital elevation model to calculate the potential annual heat load (Eq. 8 at each pixel, which is an integrated measure of latitude, slope, and a folding transformation of aspect about the northeast-southwest

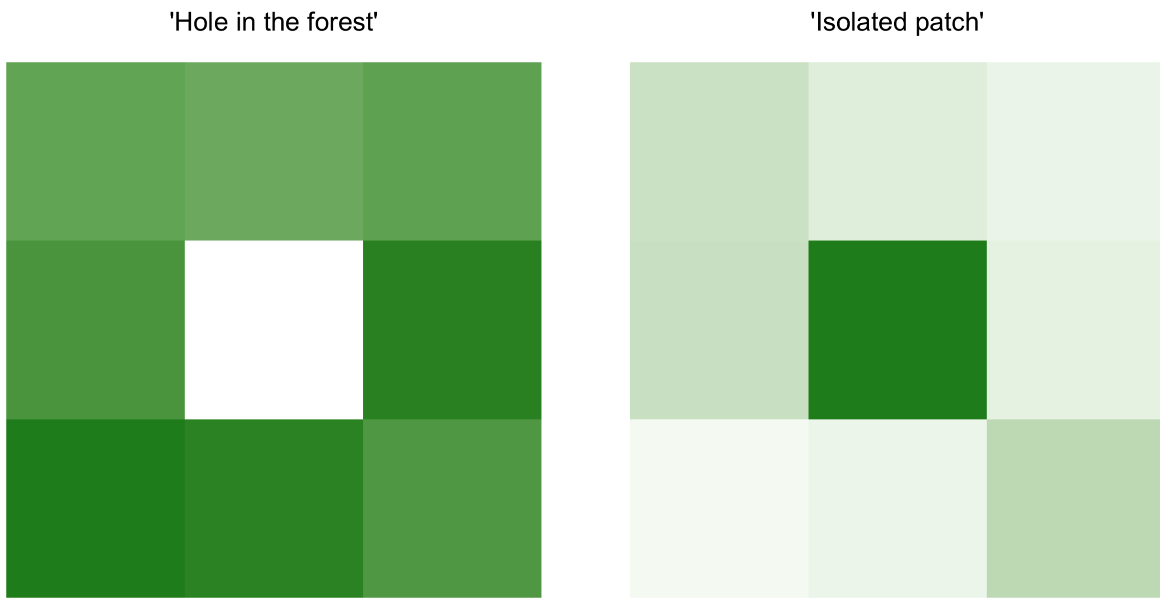

Figure 2: Conceptual diagram of 'decoupling' that sometimes occurs between the central pixel NDVI and the neighborhood mean NDVI. In each of these scenarios, our model results suggest that the probability that the central pixel burns at high severity is higher than expected given the additive effect of the covariates. The left panel depicts the "hole in the forest" decoupling, which occurs more frequently, and the right panel depicts the "isolated patch" decoupling.

line, such that northeast becomes 0 radians and southwest becomes π radians (12, 13):

$$
\begin{aligned}
aspect_{folded} &= |\pi - |aspect - \frac{5\pi}{4}|| \\
&\quad - 1.467+ \\
&\quad 1.582 * cos(latitude)cos(slope)- \\
log(pahl) &= 1.5 * cos(aspect_{folded})sin(slope)sin(latitude)- \\
&\quad 0.262 * sin(lat)sin(slope)+ \\
&\quad 0.607 * sin(aspect_{folded})sin(slope)
\end{aligned} \tag{8}
$$

Where $pahl$ is the potential annual heat load, $aspect_{folded}$ is a transformation of aspect in radians, and both $latitude$ and $slope$ are extracted from a digital elevation model with units of radians.

1. Rouse JW, Hass RH, Schell J, Deering D (1973) Monitoring vegetation systems in the great plains with ERTS. *Third Earth Resources Technology Satellite (ERTS) symposium* 1:309–317.

2. Gao BC (1996) NDWI - A normalized difference water index for remote sensing of vegetation liquid water from space. *Remote Sensing of Environment* 58(3):257–266.

3. Huesca M, García M, Roth KL, Casas A, Ustin SL (2016) Canopy structural attributes derived from AVIRIS imaging spectroscopy data in a mixed broadleaf/conifer forest. *Remote Sensing of Environment* 182:208–226.

4. García MJL, Caselles V (1991) Mapping burns and natural reforestation using thematic mapper data. *Geocarto International* 6(1):31–37.

5. Key CH, Benson NC (2006) Landscape assessment: Sampling and analysis methods. *USDA Forest Service General Technical Report RMRS-GTR-164-CD* (June):1–55.

6. USGS (2017) Product Guide: Landat 8 Surface Reflectance Code (LaSRC) Product. *USGS Professional Paper* 4.2.

7. USGS (2017) Product Guide: Landsat 4-7 Surface Reflectance (LEDAPS) Product. *USGS Professional Paper* 8(1):38.

8. Hawbaker TJ, et al. (2017) Mapping burned areas using dense time-series of Landsat data. *Remote Sensing of Environment* 198:504–522.

9. Miller JD, Thode AE (2007) Quantifying burn severity in a heterogeneous landscape with a relative version of the delta Normalized Burn Ratio (dNBR). *Remote Sensing of Environment* 109:66–80.

10. Reilly MJ, et al. (2017) Contemporary patterns of fire extent and severity in forests of the Pacific Northwest, USA (1985-2010). *Ecosphere* 8(3). doi:10.1002/ecs2.1695.

11. Parks SA, Dillon GK, Miller C (2014) A new metric for quantifying burn severity: The relativized burn ratio. *Remote Sensing* 6(3):1827–1844.

12. McCune B, Keon D (2002) Equations for potential annual direct incident radiation and heat load. *Journal of Vegetation Science* 13(1966):603–606.

13. McCune B (2007) Improved estimates of incident radiation and heat load using non-parametric regression against topographic variables. *Journal of Vegetation Science* 18(2002):751–754.